Proceedings of the 17th World Congress
The International Federation of Automatic Control
Seoul, Korea, July 6-11, 2008

Position Tracking Control with Velocity from Accelerometer and Encoder

Wen-Hong Zhu * **Tom Lamarche** *

* *Spacecraft Engineering, Canadian Space Agency*
6767 route de l'Aeroport, Saint-Hubert, QC, Canada J3Y 8Y9
(Tel: 450-926-5177; e-mails: Wen-Hong.Zhu@space.gc.ca,
Tom.Lamarche@space.gc.ca)

Abstract:
Being widely used in industrial systems and manufacturing lines, precision position control systems need to use high feedback control gains to reject disturbances. However, phase-lag in velocity estimation resulting from encoder measurement imposes a limitation on maximum allowable feedback gains, when system stability and control smoothness are concerned. In this paper, use of velocities derived from both acceleration and position measurements is suggested. The derived velocity possesses a much higher bandwidth without having theoretical phase-lag. Experimental results reveal that the use of velocities derived from practical accelerometers and encoders allows a typical position control system to substantially increase its feedback gains without compromising stability and control smoothness. It in turn results in much smaller tracking errors, compared to scenarios when velocities are created from position sensors only.

Keywords: Velocity estimation, Accelerometer; Control precision; Position control; Motion control; High-gain feedback; High accuracy pointing; Manufacturing plant control; Data-fusion; Multi-sensor systems; Estimation algorithms.

1. INTRODUCTION

Position servo control is a fundamental technology in both feed drives and robotics. Some representative works can be found in Tomizuka (1987), Zhu et al. (1992), Yao et al. (1997), Van Brussel and Van den Braembussche (1998), Pritschow (1998), Altintas et al. (2000), Renton and Elbestawi (2000), and Zhu et al. (2001).

The objective of a position control system is to make the position of a plant track its desired trajectory as precise as possible. No matter how accurate a plant model can be produced, system uncertainties always exist. Given system uncertainties, the solution for achieving high-accuracy position control is to use high feedback gains. Let

$$ms^2x(s) + f(s) + d(s) = u(s) \tag{1}$$

be a SISO point-mass plant in s-domain (Laplace transform), where m is the plant mass, x denotes the plant position, f denotes the known dynamics, d represents the plant uncertainty, and u denotes the control input.

For a given referenced (desired) trajectory x_d with bounded second-order time derivative, a typical position control law ensuring precise position tracking control can be found in Zhu et al. (1992), Altintas et al. (2000), and Zhu et al. (2001) as

$$v_r = \dot{x}_d(t) + \lambda[x_d(t) - x(t)] \tag{2}$$

$$u(t) = m\dot{v}_r(t) + f(t) + k_p[v_r(t) - v(t)] + k_I \int [v_r(t) - v(t)]dt \tag{3}$$

where $v = \dot{x}$ denote the velocity of the plant, $\lambda > 0$, $k_p > 0$, and $k_I > 0$ are three control gains, and v_r is named the *required velocity* of the plant.

Substituting (2) and (3) into (1) yields

$$m[\dot{v}_r(t) - \dot{v}] + k_p[v_r(t) - v(t)] + k_I \int [v_r(t) - v(t)]dt = d(t) \tag{4}$$

which can be further written as

$$(ms + k_p + k_I/s)[v_r(s) - v(s)] = d(s) \tag{5}$$

or

$$(ms^2 + k_p s + k_I)(s + \lambda)[x_d(s) - x(s)] = sd(s). \tag{6}$$

Remark 1. The theoretical transfer function from the desired position x_d to the actual position x exactly equals *one* with a unlimited bandwidth that is independent from the control gains. This is the unique advantage of using control laws (2) and (3) with respect to any point-mass SISO plant described by (1).

Remark 2. Many industrial systems can be modeled as point-mass SISO systems, such as single-axis motor drives, linear drives, and actuated axes in any Cartesian-type robot.

Equation (6) indicates that for given uncertainty d the position tracking error $x_d - x$ is directly affected by control gains within the frequency range specified by

$$\omega \in \left[0, \max\{\lambda, \sqrt{k_I/m}\}\right]. \tag{7}$$

Therefore, the solution to minimizing position tracking error is to use the highest possible feedback gains λ, k_I, and k_p. By doing so, however, the control smoothness and system stability are compromised. Therefore, finding the highest allowable control gains that guarantee stability is a critical task in controller tuning, see Zhu and De Schutter (2002), Zhu and Piedboeuf (2005), and Zhu et al. (2006) for examples.

In this paper, it is revealed that the way of creating velocity $v(t) = \dot{x}(t)$ has a substantial impact on the highest allowable control gains to be used. In the next section, the motivation of using high-bandwidth velocities in position control is discussed, and an approach of estimating velocity from a combination of both accelerometer and encoder is presented. In section 3, experimental results demonstrate that the position tracking error can be reduced by an order of magnitude with smoother controls, when the novel velocity estimation approach is engaged.

2. VELOCITY ESTIMATION FROM ACCELEROMETER AND ENCODER

A common practice of obtaining velocity is using either a position sensor or a tachometer. Regardless of various versions of variation, the velocity numerically generated from position measurements can be representatively written as

$$\frac{x(k) - x(k-1)}{T}$$

where $x(k)$ denotes the position measurement by an encoder at the sampling time k and T denotes the sampling period. Due to the problem's nature, the quantization error of the derived velocity is proportional to the sampling frequency. For a 1000 (Hz) sampling rate, the quantization error of the velocity in SI unit is 1000 times larger than the original quantization error of the encoder. This observation suggests a 10-bit resolution-reduction in velocity estimation. In an effort to reduce this quantization error, a low pass filter is commonly employed, which, in turn, causes very undesirable phase-lag in the estimated velocity. The same issue of phase-lag occurs when the velocity signal is measured from a tachometer, and again filtered to reduce measurement noise.

Alternatively, accelerometers measure acceleration signals that have a 90-degree phase lead over the corresponding velocity signals. An apparent way to generate velocities from accelerometer signals is through integration. However, this approach is very prone to uncertainties at low frequencies, such as the gain uncertainty and the offset, which can result in unbounded errors through integration.

In this paper, velocity estimation with high-bandwidth is concerned. An approach using a combination of both imperfect accelerometer and encoder, developed by Zhu and Lamarche (2007) for the first time in publications, is applied to position tracking control. This approach uses a frequency shaping technique to recover velocity from both acceleration and position measurements through two independent frequency-weighted channels. Parameter adaptation mechanism can be applied to update the gain of the accelerometer by projecting the acceleration signal onto the encoder signal channel.

In the following development, the Laplace transform is applied to transfer a time-domain signal to its representative signal in s-domain. Define

$$y(s) = \mathcal{L}\left(y(t)\right)$$

and

$$y(t) = \mathcal{L}^{-1}\left(y(s)\right)$$

where operator $\mathcal{L}$ denotes the Laplace transform.

Without abusing of notation, $y(s)$ can be expressed as $\left(y(t)\right)(s)$, and $y(t)$ can be expressed as $\left(y(s)\right)(t)$ throughout this paper.

2.1 Two-Channel Approach with Known Accelerometer Gain

The output of an accelerometer can be expressed as

$$a^*(t) = k_a \ddot{x}(t) + c \tag{8}$$

where $a^*(t)$ denotes the output of the accelerometer, k_a is its gain, while $x(t)$ denotes the position, and c denotes the offset.

An intuitive approach to remove the offset is to apply a high-pass filter

$$H(s) = \frac{s}{s + k_1} \tag{9}$$

where k_1 is a small positive number characterizing the bypass frequency.

Note that the intuitive approach of obtaining the velocity from the acceleration is through a pure integral operation $1/s$. Consider the fact that the integral operation possesses an infinite gain at zero frequency. Therefore, a low-pass filter

$$L(s) = \frac{k_2}{s + k_2} \tag{10}$$

is used instead, where $k_2 > 0$ determines the cut-off frequency of the low-pass filter. The low-pass filter is used as an integrator. Therefore, unlike the usual course, the low-pass filter in this paper comes into play for frequencies beyond its cut-off frequency. Consequently, the velocity obtained from the accelerometer channel in s-domain is

$$\begin{aligned} v_1^*(s) &= \frac{1}{k_2 k_a} L(s) H(s) a^*(s) \\ &= \frac{s^2}{s^2 + (k_1 + k_2)s + k_1 k_2} sx(s) \end{aligned} \tag{11}$$

where v_1^* represents the velocity extracted purely from the accelerometer.

When $k_1 \to 0$ and $k_2 \to 0$, it gives $v_1^*(s) \to sx(s) = v(s)$ as expected. However, practical concerns stated early prevent $k_1 \to 0$ and $k_2 \to 0$ from being used. Therefore, a second channel from the encoder is used as

$$v_2^*(s) = F(s) x^*(s) \tag{12}$$

to make up the difference between $v_1^*(s)$ and the true velocity $sx(s) = v(s)$, where

$$F(s) = (k_1+k_2) + \frac{[k_1k_2-(k_1+k_2)^2]s-(k_1+k_2)k_1k_2}{s^2+(k_1+k_2)s+k_1k_2} = \frac{(k_1+k_2)s+k_1k_2}{s^2+(k_1+k_2)s+k_1k_2}s \quad (13)$$

$$x^*(s) = x(s)+\delta(x) \quad (14)$$

and $x^*(s)$ denotes the position measurement in s-domain and $\delta(x)$ denotes the quantization error of the encoder.

When a perfect encoder is used with $\delta(x)=0$, substituting (13) and (14) into (12) yields

$$v^*(s) \triangleq v_1^*(s)+v_2^*(s) = v(s). \quad (15)$$

Remark 3. With a relatively high resolution encoder, $\delta(x)\to 0$ can be obtained.

Theorem 1. With an accelerometer (8) and an encoder (14), the velocity estimate obtained from (9)-(13), and (15) gives the true velocity provided that $\delta(x)=0$. ■

Remark 4. In view of (11)-(15), it can be concluded that the frequency weightings of the position and acceleration channels are determined by the two parameters k_1 and k_2. Roughly speaking, in the frequency range from zero to k_1, the encoder fully contributes to the velocity estimation with the accelerometer being less significant. In the frequency range from k_1 to k_2, both devices play a part. For frequencies beyond k_2, the accelerometer fully contributes to the velocity estimation.

2.2 Adaptive Mechanism for Unknown Accelerometer Gain

Eqs. (11) and (12) define two frequency-weighted channels to estimate the true velocity under two assumptions that the encoder resolution is sufficiently high and that the acceleration gain of the accelerometer is known. While having an encoder with a sufficient resolution is commercially possible, having a solid-state accelerometer with known acceleration gain is very difficult, if not impossible, since solid-state devices always demonstrate signal drift with time and temperature. A solution is to use an adaptive mechanism to estimate the gain of the accelerometer online. To this end, Eq. (11) is rewritten as

$$v_{1a}^*(t) = \hat{\xi}(t)\frac{1}{k_2}\left(L(s)H(s)a^*(s)\right)(t) = k_a\hat{\xi}(t)\left(\frac{s^2}{s^2+(k_1+k_2)s+k_1k_2}sx(s)\right)(t) \quad (16)$$

where $\hat{\xi}(t)$ denotes the estimate of $1/k_a$, and is governed by

$$\dot{\hat{\xi}}(t) = \mathcal{P}\left(-e(t)(L(s)H(s)a^*(s))(t),\gamma,\xi^-,\xi^+\right) \quad (17)$$

$$e(s) \stackrel{def}{=} \frac{\lambda_c}{s+\lambda_c}\left(v_{1a}^*(s)+v_2^*(s)\right)-\frac{\lambda_c s}{s+\lambda_c}x^*(s) = \frac{\lambda_c}{s+\lambda_c}\left[(v_{1a}^*(s)+v_2^*(s))-v(s)-s\delta\right] \quad (18)$$

where $\lambda_c>0$ is a constant defining a low-pass filter which gives the filtered velocity error signal denoted as e, and the $\mathcal{P}$ function is defined in Appendix A with $\gamma>0$ being the update gain and ξ^- and ξ^+ being the lower and upper bounds of $\xi = 1/k_a$. In (17), the first argument of $\mathcal{P}$ is used to drive $\dot{\hat{\xi}}$ with the update gain specified by the second argument, within the range specified by the third and fourth arguments. It can be seen from the definition of the $\mathcal{P}$ function in Appendix A that

$$(\xi-\hat{\xi}(t))\left\{-\gamma e(t)(L(s)H(s)a^*(s))(t)-\dot{\hat{\xi}}(t)\right\}\le 0. \quad (19)$$

Note that e in (18) denotes the filtered velocity estimation error based on the fact that the filtered velocity can be obtained from the encoder. When $\delta(x)=0$, substituting (11), (15), and (16) into (18) yields

$$e(s) = -\frac{\lambda_c}{s+\lambda_c}\frac{1}{k_2}\left(\left(L(s)H(s)a^*(s)\right)(t)[\xi-\hat{\xi}(t)]\right)(s) \quad (20)$$

which is equivalent to

$$\dot{e}(t) = -\lambda_c e(t)-\frac{\lambda_c}{k_2}\left(L(s)H(s)a^*(s)\right)(t)\left(\xi-\hat{\xi}(t)\right). \quad (21)$$

It can be clearly seen that the filtered velocity error e is directly related to the accelerometer gain estimation error $\xi-\hat{\xi}(t)$, and e is also used to drive $\dot{\hat{\xi}}$ through the $\mathcal{P}$ function defined by (17).

The asymptotic stability of $e(t)$ is necessary for the convergence of $\xi-\hat{\xi}$. To make this objective work, a non-negative function is defined as

$$V_a(t) = \frac{1}{2}\left[e(t)^2+\frac{\lambda_c}{k_2\gamma}(\xi-\hat{\xi}(t))^2\right]. \quad (22)$$

In view of (19) and (21), the time derivative of (22) can be written as

$$\begin{aligned}\dot{V}_a(t) &= e(t)\dot{e}(t)-\frac{\lambda_c}{k_2\gamma}(\xi-\hat{\xi}(t))\dot{\hat{\xi}}(t)\\ &= e(t)\left[-\lambda_c e(t)-\frac{\lambda_c}{k_2}\left(L(s)H(s)a^*(s)\right)(t)\left(\xi(t)-\hat{\xi}(t)\right)\right]-\frac{\lambda_c}{k_2\gamma}(\xi-\hat{\xi}(t))\dot{\hat{\xi}}(t)\\ &= -\lambda_c e(t)^2+\frac{\lambda_c}{k_2\gamma}(\xi-\hat{\xi}(t))\left[-\gamma e(t)\left(L(s)H(s)a^*(s)\right)(t)-\dot{\hat{\xi}}(t)\right]\\ &\le -\lambda_c e(t)^2. \end{aligned} \quad (23)$$

In view of (22), integrating (23) over time yields

$$e(t)\in L_\infty\bigcap L_2 \quad (24)$$

$$\xi-\hat{\xi}(t)\in L_\infty. \quad (25)$$

The boundedness of $a^*(t)$ leads to the boundedness of $\left(L(s)H(s)a^*(s)\right)(t)$ and the boundedness of $\frac{d}{dt}\left(L(s)H(s)a^*(s)\right)(t)$, which further lead to the boundedness of both $\dot{e}(t)$ and $\ddot{e}(t)$, in view of (9), (10), (21) and its time derivative, and (24). It follows from Lemmas B1 and B2 in Appendix B that

$$e(t) \to 0 \tag{26}$$

$$\dot{e}(t) \to 0 \tag{27}$$

when the acceleration output is bounded.

Re-write (18) in time-domain as

$$\dot{e}(t) + \lambda_c e(t) = \lambda_c \left[(v_{1a}^*(t) + v_2^*(t)) - v(t) - \dot{\delta}(t) \right]. \tag{28}$$

When the encoder quantization error is negligible with $\delta(x) = 0$ and $\dot{\delta}(t) = 0$, it follows from (26) and (27) that

$$v_{1a}^*(t) + v_2^*(t) \to v(t). \tag{29}$$

Theorem 2. With an accelerometer (8) and an encoder (14), the velocity estimate obtained from (9), (10), (16)-(18), and (12)-(14) yields an asymptotic estimation of the true velocity in the sense of (29) provided that $a^*(t) \in L_\infty$ and $\delta(x) = 0$. ■

Bounded accelerometer output $a^*(t) \in L_\infty$ and negligible encoder quantization error $\delta(x) = 0$ lead to (26) and (27). Thus, In view of (21), the asymptotic convergence of the parameter error

$$\xi - \hat{\xi}(t) \to 0 \tag{30}$$

requires $(L(s)H(s)a^*(s))(t) \neq 0$ or $v_{1a}^*(t) \neq 0$, $\forall t$, that is, the output of the acceleration channel is not zero.

Theorem 3. The parameter adaptation law (17), together with (8)-(10) and (18), yields an asymptotic estimation of the true parameter $\xi = 1/k_a$ in the sense of (30) provided that $a^*(t) \in L_\infty$, $v_{1a}^*(t) \neq 0$, $\forall t$, and $\delta(x) = 0$. ■

3. EXPERIMENTS

The experimental setup is photographed in Fig 1 with a drawing in Fig 2. A rail-guided mass is driven by a brushless motor through two cranks with $l = 0.0983$ (m). The mass is permitted to move horizontally without subject to gravity. A linear encoder with a resolution of one-micron is used to measure the linear position $x(t)$ and a motor attached encoder is used to measure the motor angle $q(t)$. The trigonometric structure gives

$$\dot{x}(t) = \frac{-x(t) l \sin(q(t))}{x(t) - l\cos(q(t))} \dot{q}(t) \tag{31}$$

which can also be used to relate the horizontal mass driving force to the motor torque. A real-time control system with a sampling rate of 1000 (Hz) is used.

The experimental results of using the velocity estimated from (8)-(10), (16)-(18), and (12)-(14) are demonstrated in Figs. 3 and 4. The filter parameters $k_1 = 0.1$ (1/s) and $k_2 = 20$ (1/s) are used. One percent of accelerometer gain uncertainty is assumed, leading to $\xi^- = 0.99$, $\xi^+ = 1.01$ in (17), while the parameter adaptation gain $\gamma = 1$ (s/m^2) is chosen. The desired position trajectory is designed as

$$x_d(t) = 0.008 \sin(5t) + 0.1346 \text{ (m)}. \tag{32}$$

In Fig. 3, the upper plot represents the position tracking error and the lower plot represents the control force. In Fig. 4, the upper figure shows the estimated velocity (solid line) versus the desired velocity (dashed line). The lower figure shows the accelerometer gain adaptation. The

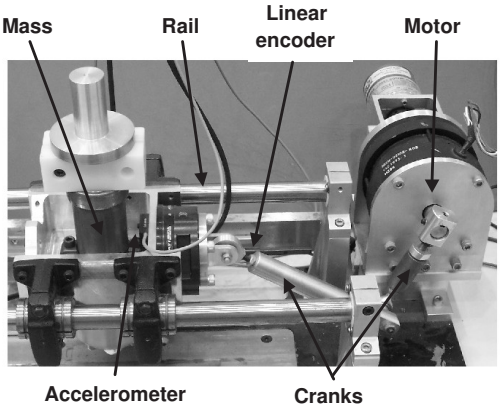

Fig. 1. Experimental setup.

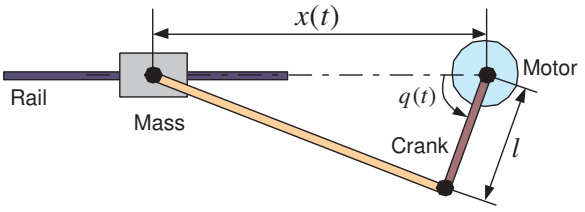

Fig. 2. Setup drawing.

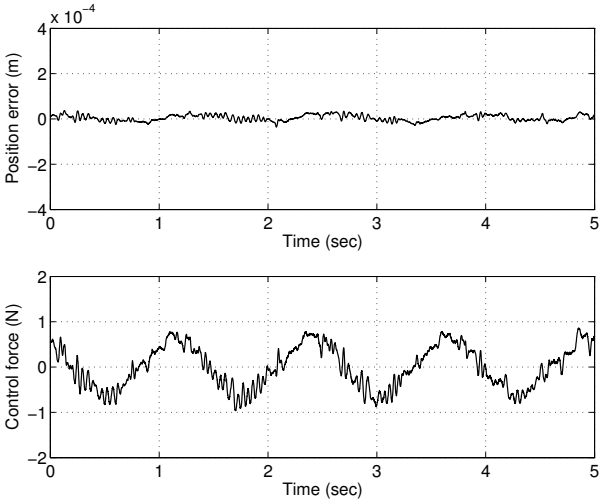

Fig. 3. Position control by using velocity from an accelerometer and an encoder.

estimated accelerometer gain is relatively stable within the range from 1.0021 to 1.0022 (about 0.01% in variation).

Remark 5. The desired trajectory given in (32) is a sinusoidal signal. The frequency is randomly selected without compromising the generality. It is expected that the responses to trajectories comprised of multiple sinusoidal inputs will be quite similar.

In Figs. 5 and 6, experimental results of using the velocity estimated from an encoder through

$$v(s) = \frac{200s}{s + 200} x(s)$$

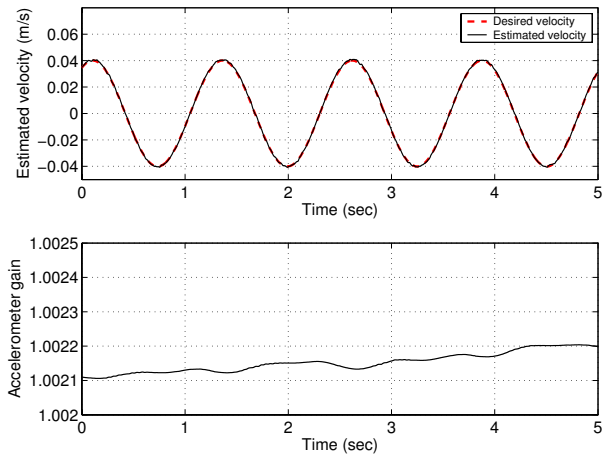

Fig. 4. Velocity estimation and accelerometer gain adaptation corresponding to Fig. 3.

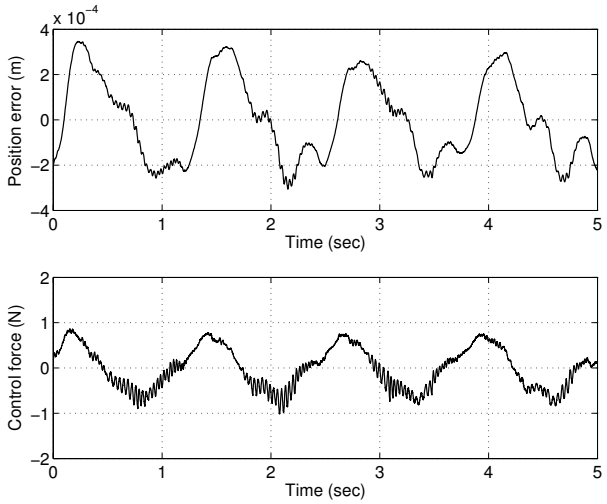

Fig. 5. Position control by using velocity from an encoder with lower control gains.

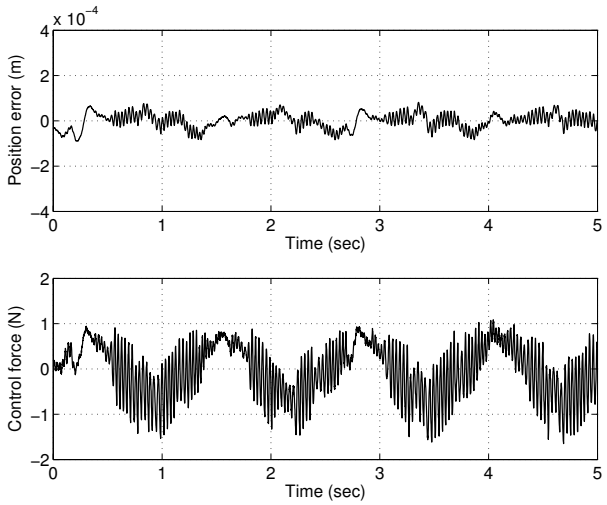

Fig. 6. Position control by using velocity from an encoder with higher control gains.

Table 1. Control parameters and position tracking results.

	Velocity from accelerometer and encoder	Velocity from encoder	
Figures	Fig. 3	Fig. 5	Fig. 6
λ (1/s)	40	10	20
k_p (Ns/m)	200	50	100
k_I (N/m)	5000	500	2000
m (kg)	3.0	3.0	3.0
$\sqrt{k_I/m}$ (1/s)	40.8	12.9	25.8
$\max \lvert e \rvert$ (m)	3.72×10^{-5}	3.46×10^{-4}	9×10^{-5}

in s-domain or

$$v(k) = \frac{200(z-1)}{z-0.8} x(k)$$

in z-domain are presented. Lower control gains are used in Fig. 5, and higher control gains are used in Fig. 6 . The control parameters corresponding to Figs. 3 to 6 are summarized in Table 3.

In view of Fig. 3 and Fig. 5, the position tracking error is reduced by about an order of magnitude with comparable control smoothness. In view of Fig. 3 and Fig. 6, both advantages of having smaller position tracking error and smoother control are shown. It is clear that the use of velocity from both accelerometer and encoder allows a motion controller to use much higher feedback gains without compromising the control smoothness. Consequently, the use of higher control gains substantially reduce the position tracking error (about an order of magnitude depending on the system).

Remark 6. Compared to velocities estimated from encoders along, velocities estimated from both position and acceleration sensors are having faster responses, much less phase lags, and much smoother profiles. An example has been given in Zhu and Lamarche (2007).

4. CONCLUSION

High-bandwidth velocities derived from both acceleration and position sensors are suggested to be used in position tracking control of industrial plants. The use of the suggested velocity estimation allows a typical position controller to substantially increase its control gains leading to much smaller position tracking errors without compromising control smoothness, as demonstrated in the experiments.

REFERENCES

Y. Altintas, K. Erkorkmaz, and W.-H. Zhu. Sliding mode controller design for high speed feed drives. *Annals of CIRP*, 49(1):265–270, 2000.

K. S. Narendra and L. S. Valavani. A comparison of Lyapunov and hyperstability approaches to adaptive control of continuous systems. *IEEE Trans. Automatic Control*, 25(2):243-247, 1980.

G. Pritschow. A comparison of linear and conventional electromechanical drives. *Annals of CIRP*, 47(2):541–548, 1998.

D. Renton and M. A. Elbestawi. High speed servo control of multi-axis machine tools. *Int. J. Machine Tools and Manufacture*, 40(4):539–559, 2000.

G. Tao. A simple alternative to the Barbălat lemma. *IEEE Trans. Automatic Control*, 42(5):698, 1997.

M. Tomizuka. Zero phase error tracking algorithm for digital control. *ASME J. Dynamic Systems, Measurement, and Control*, 109:65–68, 1987.

H. Van Brussel and P. Van den Braembussche. Robust control of feed drives with linear motors. *Annals of CIRP*, 47(2):325–328, 1998.

B. Yao, M. Al-Majed, and M. Tomizuka. High-performance robust motion control of machine tools: an adaptive robust control approach and comparative experiments. *IEEE/ASME Trans. Mechatronics*, 2(2):63–76, 1997.

W.-H. Zhu, H.-T. Chen, and Z.-J. Zhang. A variable structure robot control algorithm with an observer. *IEEE Trans. Robotics and Automation*, 8(4):486–492, 1992.

W.-H. Zhu and J. De Schutter. Adaptive control of mixed rigid/flexible joint robot manipulators based on virtual decomposition. *IEEE Trans. Robotics and Automation*, 15(2):310–317, 1999.

W.-H. Zhu, and S. E. Salcudean. Stability guaranteed teleoperation: an adaptive motion/force control approach. *IEEE Trans. Automatic Control*, 45(11):1951–1969, 2000.

W.-H. Zhu, M.B. Jun, and Y. Altintas. A fast tool servo design for precision turning of shafts on conventional CNC lathes. *Int. J. Machine Tools & Manufacture*, 41(7):953–965, 2001.

W.-H. Zhu and J. De Schutter. Experimental verifications of virtual decomposition based motion/force control. *IEEE Trans. Robotics and Automation*, 18(3):379–386, 2002.

W.-H. Zhu and J.-C. Piedboeuf. Adaptive output force tracking control of hydraulic cylinders with applications to robot manipulators. *ASME J. Dynamic Systems, Measurement, and Control*, 127(2):206–217, June 2005.

W.-H. Zhu, E. Dupuis, M. Doyon, J.-C. Piedboeuf. Adaptive control of harmonic drives based on virtual decomposition. *IEEE/ASME Trans. Mechatronics*, vol. 11(5):604–614, October 2006.

W.-H. Zhu and T. Lamarche. Velocity estimation by using position and acceleration sensors. *IEEE Trans. Industrial Electronics*, 54(5):2706–2715, 2007.

Appendix A. $\mathcal{P}$ FUNCTION FOR PARAMETER ADAPTATION

The $\mathcal{P}$ function defined in (Zhu and De Schutter, 1999, page 311) takes the following form:

Definition A1. $\mathcal{P}(s(t), k, a, b) \in R$ is a differentiable scalar function, where $s(t) \in R$ is a scalar variable and k, a, b are three constants with $k > 0$, $a \leq b$, such that

$$\dot{\mathcal{P}} = k s(t) \kappa \tag{A.1}$$

$$\text{with } \kappa = \begin{cases} 0 & \mathcal{P} \leq a \ \& \ s(t) \leq 0 \\ 0 & \mathcal{P} \geq b \ \& \ s(t) \geq 0 \\ 1 & \text{otherwise} \end{cases}.$$

Lemma A1.: Consider a $\mathcal{P}$ function defined by (A.1). For any scalar $\mathcal{P}^*$ with $a \leq \mathcal{P}^* \leq b$, it follows that

$$(\mathcal{P}^* - \mathcal{P}) \left(s(t) - \frac{1}{k} \dot{\mathcal{P}} \right) \leq 0. \tag{A.2}$$

■

Appendix B. MATHEMATICAL LEMMAS

The following lemma is from Tao (1997).

Lemma B1. If $\epsilon(t) \in L_2$ and $\dot{\epsilon}(t) \in L_\infty$, then $\lim_{t\to\infty} \epsilon(t) = 0$. ■

The following lemma is from Narendra and Valavani (1980).

Lemma B2. If g is a real function of the real variable t defined and uniformly continuous for $t > 0$ and if the limit of the integral

$$\int_0^t g(\tau) d\tau$$

as t tends to infinity exists and is a finite number, then

$$\lim_{t\to\infty} g(t) = 0.$$

■